NeuroImage: Clinical 18 (2018) 103–114

Contents lists available at ScienceDirect

NeuroImage: Clinical

journal homepage: www.elsevier.com/locate/ynicl

Cortical folding alterations in fetuses with isolated non-severe ventriculomegaly

Oualid M. Benkarim[a], Nadine Hahner[b,c], Gemma Piella[a], Eduard Gratacos[b,c], Miguel Angel González Ballester[a,d], Elisenda Eixarch[b,c,*], Gerard Sanroma[a]

[a] DTIC, Universitat Pompeu Fabra, Barcelona, Spain
[b] Fetal i+D Fetal Medicine Research Center, BCNatal — Barcelona Center for Maternal-Fetal and Neonatal Medicine (Hospital Clínic and Hospital Sant Joan de Deu), Institut Clínic de Ginecologia, Obstetricia i Neonatologia, IDIBAPS, Universitat de Barcelona, Barcelona, Spain
[c] Centre for Biomedical Research on Rare Diseases (CIBER-ER), Barcelona, Spain
[d] ICREA, Barcelona, Spain

ARTICLE INFO

Keywords:
Fetal brain
MRI
Ventriculomegaly
Cortical folding
Statistical analysis
Lasso

ABSTRACT

Neuroimaging of brain diseases plays a crucial role in understanding brain abnormalities and early diagnosis. Of great importance is the study of brain abnormalities *in utero* and the assessment of deviations in case of maldevelopment. In this work, brain magnetic resonance images from 23 isolated non-severe ventriculomegaly (INSVM) fetuses and 25 healthy controls between 26 and 29 gestational weeks were used to identify INSVM-related cortical folding deviations from normative development. Since these alterations may reflect abnormal neurodevelopment, our working hypothesis is that markers of cortical folding can provide cues to improve the prediction of later neurodevelopmental problems in INSVM subjects. We analyzed the relationship of ventricular enlargement with cortical folding alterations in a regional basis using several curvature-based measures describing the folding of each cortical region. Statistical analysis (global and hemispheric) and sparse linear regression approaches were then used to find the cortical regions whose folding is associated with ventricular dilation. Results from both approaches were in great accordance, showing a significant cortical folding decrease in the insula, posterior part of the temporal lobe and occipital lobe. Moreover, compared to the global analysis, stronger ipsilateral associations of ventricular enlargement with reduced cortical folding were encountered by the hemispheric analysis. Our findings confirm and extend previous studies by identifying various cortical regions and emphasizing ipsilateral effects of ventricular enlargement in altered folding. This suggests that INSVM is an indicator of altered cortical development, and moreover, cortical regions with reduced folding constitute potential prognostic biomarkers to be used in follow-up studies to decipher the outcome of INSVM fetuses.

1. Introduction

Cortical folding is a major developmental process the human brain embarks on during the intrauterine period to acquire its highly gyrencephalic adult morphology. In early gestation, the cortex is a smooth sheet that becomes intensively convoluted following an ordered sequence of sulcogyral formation, with primary and secondary sulci obeying stable spatio-temporal patterns, while more irregular patterns govern the emergence of tertiary sulci. These cortical convolutions are intrinsically related to the functional organization of the cortex. Consequently, alterations in the degree and pattern of cortical folding might have a profound impact on brain function (Fernández et al., 2016). In adults, several studies have revealed associations of altered folding with functional disabilities in a wide spectrum of disorders such as schizophrenia (Jou et al., 2005) and attention-deficit/hyperactivity disorder (Wolosin et al., 2009). These functional disturbances might involve early cortical folding malformations and manifest in adulthood as symptomatic consequences of said maldevelopment (Wolosin et al., 2009; Batty et al., 2015; Rehn and Rees, 2005; Powell, 2010).

Since gyrification commences early in pregnancy, gestation constitutes a vulnerable period for cortical folding, where prenatal diagnosis of cerebral abnormalities is of paramount importance. In the fetus, ventriculomegaly (VM) is the most frequent abnormal finding in prenatal ultrasound examination and occurs in around 1% of fetuses (Salomon et al., 2007; Huisman et al., 2012). Fetal VM is a condition in which the lateral ventricles are dilated, and is defined as an atrial diameter of ≥10 mm of one or both lateral ventricles at any gestational age (GA) from 14 weeks onwards (Cardoza et al., 1988), being 6–8 mm

* Corresponding author.
E-mail address: eixarch@clinic.cat (E. Eixarch).

https://doi.org/10.1016/j.nicl.2018.01.006
Received 3 August 2017; Received in revised form 23 November 2017; Accepted 9 January 2018
Available online 28 January 2018

the width in normal fetuses. These measurements remain stable in the second and third trimesters (ISUOG Guidelines, 2007). In case of ventricular enlargement, an atrial diameter in the range of 10–15 mm constitutes non-severe VM, while a measurement larger than 15 mm refers to severe VM. Non-severe VM is further classified into mild (10–12 mm) and moderate (12–15 mm). In case of no other anomalies, it is called isolated VM.

Though studies have found associations of ventricular enlargement with attention-deficit/hyperactivity disorder (Lyoo et al., 1996) and schizophrenia (Wright et al., 2000; Vita et al., 2000), the implications of fetal VM in such disorders remain largely unclear due to scarce long-term follow-up studies and the appearance of confounding factors during development. Nevertheless, isolated non-severe ventriculomegaly (INSVM)-associated neurodevelopmental deficits have been observed in neonates and infants (Sadan et al., 2007; Leitner et al., 2009; Gómez-Arriaga et al., 2012). When VM is diagnosed, postnatal prognosis is highly dependent on the presence of other abnormalities and the degree of ventricular dilation (Griffiths et al., 2010). There is a high risk of poor neurodevelopmental outcome when other abnormalities are diagnosed and/or the ventricles are severely dilated. However, INSVM fetuses are not so prone to have neurodevelopmental problems (Melchiorre et al., 2009; Griffiths et al., 2010), and the ones that will have unfavorable outcome cannot be characterized solely by the atrial diameter (Beeghly et al., 2010). With altered cortical folding found in fetuses with INSVM (Scott et al., 2013), the assessment of cortical folding can play an important role in prognosis reliability (Li et al., 2011).

Although ultrasound is the most used imaging modality for evaluating pregnancies, VM is a common indication for fetal magnetic resonance imaging (MRI) (Rutherford, 2001). Indeed, MRI of the *in vivo* fetal brain has recently attracted increasing attention from the neuroscientific community and is becoming an important tool in the study of *in utero* brain development (Benkarim et al., 2017; Studholme and Rousseau, 2014). There are several works in the literature that use 3D MRI to investigate the intrauterine cerebral growth in healthy populations (Habas et al., 2012; Clouchoux et al., 2012; Wright et al., 2014, 2015). These neuroimaging studies attempt to identify and set the normative morphological and functional changes the fetal brain undergoes during its maturational course. On the other hand, neuroimaging of diseased brains provides the means to find disease-specific deviations from the aforementioned normative development and the discovery of stable biomarkers that accurately discriminate such diseases. Using 3D reconstructed MRI, isolated VM has been previously studied in Scott et al. (2013) and Kyriakopoulou et al. (2014). Scott et al. (2013) analyzed volumetric and cortical folding differences between 16 cases and 16 controls in the age range of 22–25.5 gestational weeks (GWs). Volumetric analysis was carried out by Kyriakopoulou et al. (2014) in 60 controls and 65 cases within the GA range of 22–38 weeks. Among their findings, Kyriakopoulou et al. (2014) showed increased cortical volume in fetuses with VM, and Scott et al. (2013) found reduced cortical folding in both hemispheres, although in a narrow area near the parieto-occipital sulcus.

In this work, 3D reconstructed fetal brain MR images were used to investigate the relationship of INSVM with alterations in gyrification between a cohort of 25 healthy controls and 23 INSVM fetuses within the age range of 26–29 GWs. There are no studies that investigated cortical folding under VM in the third trimester of gestation. During this period, numerous cortical landmarks are prominently developed in the normal fetal brain (e.g., superior temporal sulcus and calcarine fissure) (Clouchoux et al., 2012), which allow susceptible deviations in gyrification to be reliably detected. Cortical folding was quantified using several curvature-based folding measures (e.g., mean curvature, shape index and curvedness). These descriptors offer a different perspective into intrauterine neurodevelopment than brain volumetry. Curvedness, for instance, was shown to provide different information and be more accurate in the prediction of GA than brain volume (Hu et al., 2013; Wu et al., 2015). With several descriptors we can, furthermore, capture different shape characteristics of the cortex. Positive and negative versions of some folding measures (e.g., positive and negative mean curvature) were further incorporated to respectively account for folding confined in gyral and sulcal areas, which affords a separate inspection of cortical folding. The cortex was parcellated in several regions to study cortical folding differences in a regional basis. Statistical analysis and sparse regression approaches were adopted to analyze folding differences related to ventricular enlargement and identify cortical regions with altered folding. The present study seeks to add to previous studies by providing insights into the gyrification alterations potentially associated with INSVM at mid-third trimester of gestation (where the majority of primary sulci are formed), assessing the relationship from different methodological approaches, and characterizing the implication of ventricular enlargement laterality in cortical alterations.

2. Materials and methods

2.1. Subjects

For our study, we included 25 healthy controls and 23 subjects diagnosed with INSVM from a larger prospective cohort of 81 subjects within a research project on congenital isolated VM. INSVM was defined as unilateral or bilateral ventricular width between 10 and 14.9 mm. All fetuses were from singleton pregnancies and met the inclusion criteria of having no abnormal karyotype, infections or malformations with risk of abnormal neurodevelopment. Approval was obtained for the study protocol from the Ethics Committee of the Hospital Clínic in Barcelona — Spain (HCB/2014/0484) and all patients gave written informed consent. Fetal MRI was performed between 26 and 29 GWs. Pregnancies were dated according to the first-trimester crown-rump length measurements (Robinson and Fleming, 1975). Table 1 presents the number of subjects and mean GA per cohort, with INSVM cases grouped by left, right or bilateral ventricular enlargement.

2.2. MRI acquisition and reconstruction

T2-weighted MR imaging was performed on a 1.5-T scanner (SIEMENS MAGNETOM Aera syngo MR D13; Munich, Germany) with a 8-channel body coil. All images were acquired without sedation and following the American college of radiology guidelines for pregnancy and lactation. Half Fourier acquisition single shot turbo spin echo (HASTE) sequences were used with the following parameters: echo time of 82 ms, repetition time of 1500 ms, number of averaging = 1, 2.5 mm of slice thickness, 280×280 mm field of view and voxel size of $0.5 \times 0.5 \times 2.5$ mm^3. For each subject, multiple orthogonal acquisitions were performed: 4 axial, 2 coronal and 2 sagittal stacks. Final 3D motion-corrected reconstructions were obtained from these 8 stacks of thick 2D slices. Brain location and extraction from 2D slices was carried out in an automatic manner using the approach proposed by Keraudren et al. (2014), followed by high-resolution 3D volume reconstruction

Table 1
Demographics. Number of subjects (*N*), mean GA and standard deviation expressed in GW, and gender (M/F, where M and F stand for male and female, respectively) per cohort. The INSVM cohort is further divided in 3 subgroups (left, right and bilateral) according to unilateral or bilateral VM diagnosis.

	N	GW	M/F
Control	25	27.6 ± 0.9	14/11
INSVM			
Bilateral	5	27.3 ± 0.9	4/1
Left	8	28.1 ± 0.8	8/0
Right	10	27.2 ± 1.0	9/1
Total	23	27.5 ± 1.0	21/2

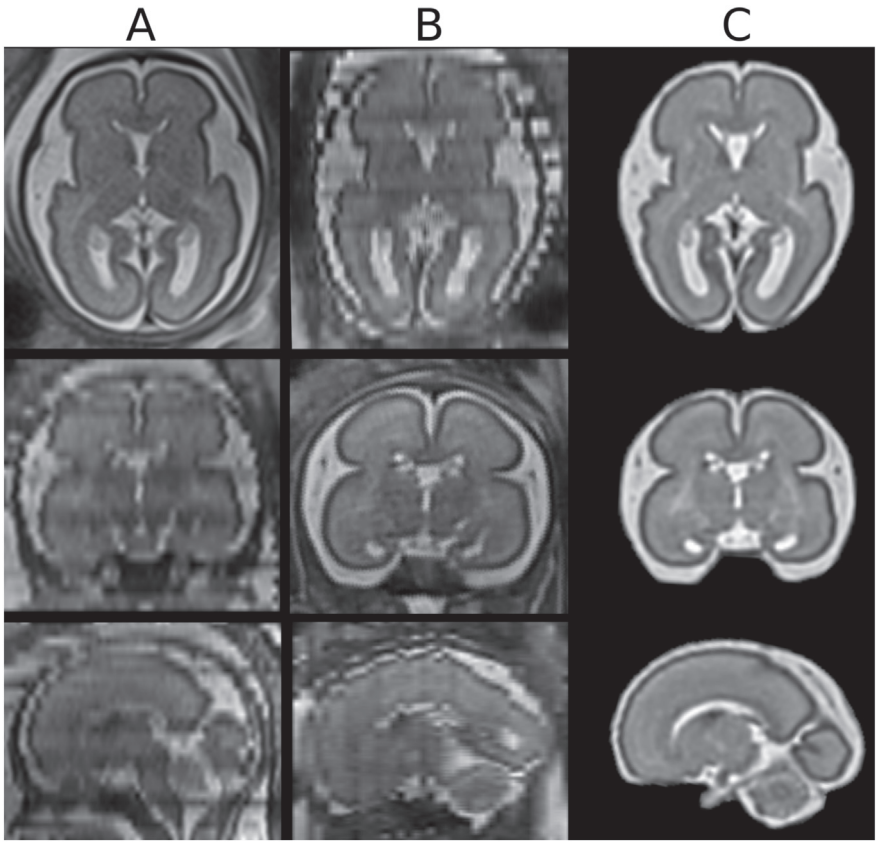

Fig. 1. Brain MRI of a 26 GW-old healthy control reconstructed from 8 stacks of 2.5 mm slice thickness. From top to bottom: axial, coronal and sagittal views of axial (A) and coronal (B) raw stacks, and final reconstruction (C).

using the method presented in Murgasova et al. (2012). Fig. 1 shows an example of 2 raw acquisitions and the final reconstructed volume.

2.3. Tissue segmentation

Reconstructed MR images were segmented with the method proposed in Sanroma et al. (2016) into white matter (WM), cortex, cerebrospinal fluid (CSF), ventricles, cerebellum and brainstem. Briefly, this is an ensemble method that learns the optimal spatial combination of a set of base methods. It is based on the hypothesis that different segmentation methods complement each other in different regions of the brain. As base segmentation methods we used joint label fusion (Wang et al., 2013) and *Atropos* (Avants et al., 2011), which were then spatially combined as proposed by Sanroma et al. (2016). Segmentations for 4 subjects, manually delineated by an expert, were used as atlases for the segmentation method. Fig. 2 displays an example of a reconstructed brain MRI and its corresponding automatic labeling.

2.4. Cortical surface extraction

To study gyrification, the inner cortical surface was chosen instead of the outer surface since the interface between WM and cortex is more stable and less prone to segmentation errors due to partial volume effects than the cortex-CSF interface. The WM binary masks were smoothed using a 2 mm full width at half-maximum Gaussian kernel and cortical surface meshes for each hemisphere were then reconstructed with the marching cubes algorithm (Lorensen and Cline, 1987).

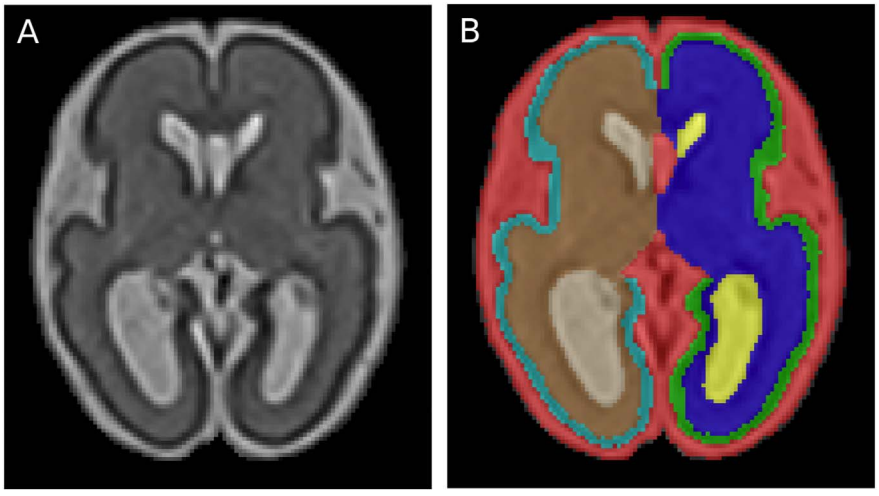

Fig. 2. Fetal brain MRI segmentation: 26.4 GW-old fetus with right INSVM (A) and corresponding segmentation (B), with different labels for left and right WM, cortex and lateral ventricles.

Table 2
Cortical regions from the neonatal atlas provided by Makropoulos et al. (2014) and their abbreviations. Each hemisphere is parcellated into these 16 cortical regions.

		Abbreviation
Cortical region	Part	
Anterior temporal lobe	Lateral	ATLlp
	Medial	ATLmp
Cingulate gyrus	Anterior	CGap
	Posterior	CGpp
Frontal lobe		FL
Gyri parahippocampalis et ambiens	Anterior	GPAap
	Posterior	GPApp
Insula		Ins
Lateral occipitotemporal gyrus, gyrus fusiformis	Anterior	LOGFap
	Posterior	LOGFpp
Medial and inferior temporal gyri	Anterior	MITGap
	Posterior	MITGpp
Occipital lobe		OL
Parietal lobe		PL
Superior temporal gyrus	Middle	STGmp
	Posterior	STGpp

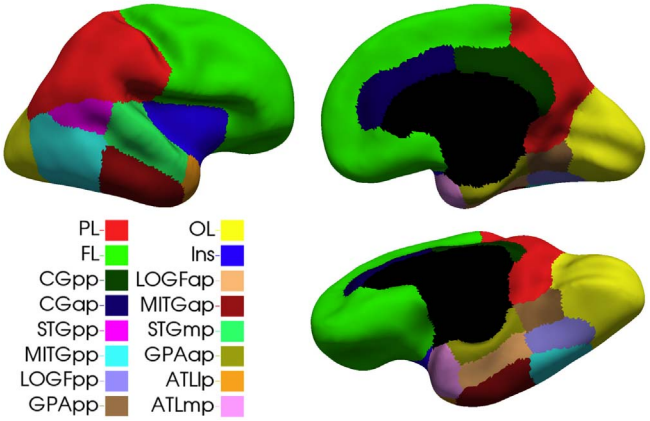

Fig. 3. Inner cortical surface parcellation.

Furthermore, a neonatal atlas with cortical regions (Makropoulos et al., 2014) was used to parcellate each hemisphere into 16 cortical regions. For each fetal brain, a neonatal atlas with a similar age was registered to it using the symmetric diffeomorphic mapping (SyN) proposed by Avants et al. (2008). Registration was performed based on intensity images and cortical masks extracted from both the fetal brain (based on the initial tissue segmentation) and the neonatal atlas (as a union of all cortical labels based on the segmentations provided by Makropoulos et al. (2014). In this way, registration is driven to provide a more accurate parcellation of the cortex. Parcellations were then visually inspected and corrected for possible mislabeling. Table 2 lists the different cortical regions and Fig. 3 shows them propagated onto the surface mesh. Cortical parcellations for all subjects are shown in supplementary material.

2.5. Regional cortical folding

Gyrification changes related to ventricular enlargement were investigated at both hemispheric and regional levels using a curvature-based approach. This approach has been previously used to study cortical folding in premature neonates (Rodriguez-Carranza et al., 2008; Shimony et al., 2016) and healthy fetuses (Wright et al., 2014; Wu et al., 2015). For each fetus, principal curvatures (i.e., k_1 and k_2) were computed at each vertex on the inner cortical surface mesh and 15 curvature-based folding measures were derived as described in Rodriguez-Carranza et al. (2008), Shimony et al. (2016), and Wright et al. (2014). Several folding measures were used in this work since a single curvature descriptor (e.g., mean curvature) may not be sufficient to fully characterize cortical folding. These measures are summarized in Table 3.

Table 3
Curvature-based folding measures used in our study. The * symbol in Eq. (1) can be substituted by any of the above curvature measures to compute the corresponding folding measure for a given cortical region. Note that superscripts $^+$ and $^-$ denote positive and negative curvature, respectively. For example, PMC is 0 in all points where $H < 0$ and H otherwise. Conversely, NMC is 0 when $H > 0$ and H otherwise. The same applies for all remaining curvatures with $^+$ and $^-$ superscripts.

	Abbreviation	Definition
Mean curvature	MC	$H = \frac{k_1 + k_2}{2}$
Positive mean curvature	PMC	H^+
Negative mean curvature	NMC	H^-
Gaussian curvature	GC	$K = k_1 k_2$
Positive Gaussian curvature	PGC	K^+
Negative Gaussian curvature	NGC	K^-
Curvedness index	CI	$C_i = \sqrt{\frac{k_1^2 + k_2^2}{2}}$
Folding index	FI	$F_i = \lvert k_1 \rvert \, (\lvert k_1 \rvert - \lvert k_2 \rvert)$
Shape index	SI	$S_i = -\frac{2}{\pi} \arctan\left(\frac{k_2 + k_1}{k_2 - k_1}\right)$
Positive shape index	PSI	S_i^+
Negative shape index	NSI	S_i^-
		$\sum_i {}^* w / \sum_i w$ (1)
Mean curvature L_2 norm	MCL2	$\sqrt{\sum_i H^2 w / \sum_i w}$
Gaussian curvature L_2 norm	GCL2	$\sqrt[4]{\sum_i K^2 w / \sum_i w}$
Mean curvature norm ratio	MCNR	$\sum_i H^2 w / \sum_i \lvert H \rvert w$
Gaussian curvature norm ratio	GCNR	$\sum_i K^2 w / \sum_i \lvert K \rvert w$

For each vertex on a surface mesh, 11 local curvature descriptors (see first 11 entries in Table 3: from MC to NSI) were computed from the principal curvatures, as shown in the third column. Then, folding for a given cortical region was characterized by a weighted average of all points belonging to such region (Eq. (1) in Table 3) for each curvature descriptor. These descriptors included MC, which is an extrinsic property of a surface created by distance preserving folding (without distortion), with positive MC values located on gyri and negative values on sulci (Schaer et al., 2008). For a given cortical region, MC denotes the overall folding of the region, while PMC only focuses on convexity (i.e., positive MC) and NMC on concavity (i.e., negative MC). On the other hand, GC is an intrinsic property of the surface that captures curvature changes created by distortion (Pienaar et al., 2008). A cortical region is ellipsoidal when the average GC is positive and saddle-shaped when negative (Van Essen and Drury, 1997). PGC and NGC summarize surface points with positive and negative GC, respectively. While jointly using the signs of MC and GC allows identifying different shapes, the SI proposed by Koenderink and van Doorn (1992) is able to capture continuous surface shapes ranging from concavity (i.e., -1) to convexity (i.e., $+1$) (Hu et al., 2013). PSI and NSI summarize region points located on gyri and sulci, respectively. Complementary to SI, Koenderink and van Doorn (1992) also proposed the CI that quantifies size by the degree of deviation of a surface from a flat plane. We also consider FI, defined as a measure of cylindrical parts of a surface (Van Essen and Drury, 1997). Four more folding measures were additionally incorporated into the analysis of gyrification (see last 4 entries in Table 3). MCL2 and GCL2 are invariant to translation, rotation and scaling, and measure bending of the surface and the amount of surface with constant Gauss curvature, respectively (Batchelor et al., 2002). MCNR and GCNR are further area independent and quantify gyrification as a ratio of curvatures (Rodriguez-Carranza et al., 2008).

The contribution of a point in the surface mesh to regional folding measures was weighted by the mean area of all cells sharing this point (w in Table 3). For all cortical folding measures used in our analyses,

the higher their values, the more folded is the cortical region, with the exceptions of the negative measures (i.e., NMC, NGC and NSI).

2.6. Statistical analysis

The aim of our study is to analyze the effect of INSVM in gyrification. Thus, to test the effect of ventricular enlargement in cortical folding, we used a general linear model (GLM) with 2 versions to characterize the changes in the aforementioned folding measures. The first model, F_D, was used to test the effect of diagnosis, as a group factor (0 for control and 1 for INSVM), and GA and supratentorial volume as covariates:

$$F_D = \beta_0 + \beta_1 GW + \beta_2 STV + \beta_3 DG, \tag{2}$$

where *GW* is GA in weeks, *DG* refers to the diagnosis, and *STV* represents supratentorial volume. The second model, F_V, uses ventricular volume as a covariate instead of diagnosis:

$$F_V = \beta_0 + \beta_1 GW + \beta_2 STV + \beta_3 VV, \tag{3}$$

where *VV* represents ventricular volume. Since the *in utero* brain becomes continuously more convoluted as growth proceeds, GA was incorporated into both models to control for the effect of age on the analyzed folding measures. Furthermore, curvature-based folding measures depend on brain size (Rodriguez-Carranza et al., 2008) and supratentorial volume (composed of WM, gray matter (GM) and ventricles) was considered as a covariate in both models to account for scaling differences (Shimony et al., 2016).

In the second model, F_V, considering ventricular volume rather than diagnosis can improve the accuracy of the model. First, because ventricular volume was found to be more distinctive in the analysis of VM than atrial diameter (Gholipour et al., 2012), and therefore more properly representative of such condition. Second, and most importantly, in fetuses with VM, ventricular dilation is not restricted to the atria (Scott et al., 2013). Instead of a dichotomous variable carrying information solely about the width of the atrium (in fact, diagnosis only tells us if the atrial width surpasses the threshold of 10 mm or not), ventricular volume is able to capture the extent of enlargement.

Besides examining folding measures at a regional level with the 2 proposed models, we further analyzed the association of lateral ventricular enlargement (using Eq. (3)) per hemisphere instead of the association of total ventricular volume with the whole cortex.

For each cortical region, 15 folding measures were extracted and tested. Results were then considered statistically significant after Bonferroni correction at $p < .05/15 \approx 0.0033$.

2.7. Sparse linear models for ventricular volume prediction

Regression models with sparsity-inducing regularization, such as the well-known Lasso (Tibshirani, 1994), are widely used in neuroimaging data analysis for diagnosis prediction and prognostic biomarker discovery (Klöppel et al., 2012; Mwangi et al., 2014; Shimizu et al., 2015). Furthermore, these approaches are well-suited for high-dimensional data, especially when the number of predictors (i.e., features) greatly exceeds the number of training samples (i.e., subjects). Our purpose is to find the most relevant cortical regions (each region is composed of 15 curvature features) in the prediction of total ventricular volume using sparse regression models. We use Lasso to enforce that the regression model will be sparse and only a portion of the predictor variables will be used in the model. This allows finding the most relevant features for the prediction of ventricular volume. By comparing these results with the ones obtained with GLM, we can draw conclusions about the cortical regions that are related to ventricular enlargement.

In our setting, each subject is represented by a 482-dimensional feature vector with 15 folding measures extracted from each of the 32 cortical regions and 2 additional features corresponding to GA and STV. Formally, let $Y \in \mathbb{R}^n$ denote a vector of total ventricular volume for all n subjects and an $n \times p$ design matrix X with the p folding measures from each subject arranged in rows. The Lasso estimator is defined as:

$$\min_{\beta} \left(\left\| Y - X\beta \right\|_2^2 + \lambda \sum_{j=1}^{p} |\beta_j| \right), \tag{4}$$

where $\beta \in \mathbb{R}^p$ is a coefficient vector, $\|\cdot\|_2^2$ is the squared Euclidean norm, λ is the penalization parameter and the second term corresponds to the l_1-norm. The first term aims at fitting the data (as in conventional regression) and the second term is the regularization for improving generalization, controlled by the λ parameter. A larger λ will force most of the features to be 0 (i.e., not selected).

Lasso is designed for selecting individual variables. In this way, we can indirectly conclude that regions with more selected features are more related to INSVM. However, our purpose is to inspect relevance at region level rather than at measure or variable level. In order to directly extract conclusions about the important regions, we can enforce Lasso to select all or none of the features from a given region. Group Lasso is an extension of Lasso that incorporates such constraint by performing selection on predefined groups of variables rather than individual variables (Yuan and Lin, 2006). Thus, all 15 folding measures corresponding to a given cortical region are considered as a group in Group Lasso regression. GA and STV are also considered separately as single feature groups. The Group Lasso estimator is defined as:

$$\min_{\beta} \left(\left\| Y - X\beta \right\|_2^2 + \lambda \sum_{l=1}^{L} \sqrt{p_l} \left\| \beta_l \right\|_2 \right), \tag{5}$$

where L is the number of groups (i.e., 34 groups: 32 cortical regions, one group for GA and another for STV), p_l is the number of variables in the l-th group and $\|\cdot\|_2$ is the Euclidean norm. When L is equal to the number of variables p, this optimization problem is equivalent to Lasso (Friedman et al., 2010).

The optimal λ values for Lasso and Group Lasso based on leave-one-out cross-validation are used to identify the most relevant cortical regions. In terms of performance in predicting the ventricular volume, it is expected that Lasso would outperform Group Lasso since Group Lasso is more constrained than Lasso in that it is forced to include or drop all measures representing a particular cortical region.

One problem with Lasso and Group Lasso is that selected (i.e., relevant) features can vary depending on the data used to compute the model. To that end, Randomized Lasso (Meinshausen and Bühlmann, 2010) determines the most stable features by randomly selecting the data used to compute the models multiple times. The Randomized Lasso estimator is defined as:

$$\min_{\beta} \left(\left\| Y - X\beta \right\|_2^2 + \lambda \sum_{j=1}^{p} \frac{|\beta_j|}{W_j} \right), \tag{6}$$

where W_j is an independent and identically distributed random variable in $[\alpha,1]$ and $\alpha \in (0,1]$ is the weakness parameter that is used to change the value of λ in Eq. (6) to be randomly chosen in the range $[\lambda,\lambda/\alpha]$. For a more detailed description, the reader is referred to the original work of Meinshausen and Bühlmann (2010).

3. Results

3.1. Ventricular volume

Total ventricular volumes for control and INSVM fetuses are shown in Fig. 4. Average total ventricular volumes were lower in healthy controls (3.65 ± 1.12 cm^3) than in INSVM fetuses (8.91 ± 2.70 cm^3). We used a GLM to analyze the association of ventricular volume with GA and diagnosis. There was a slight increase of 0.76 cm^3 ($p = .01$) in

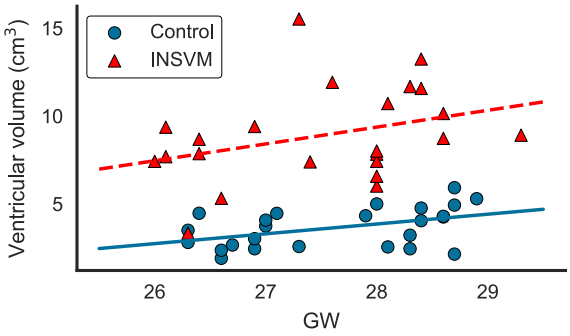

Fig. 4. Total ventricular volume with increasing GA.

ventricular volume with increasing GA. In association with diagnosis, ventricular volume was on average 5.34 cm^3 larger ($p < 10^{-20}$) in the INSVM cohort than in healthy controls, which is obvious since INSVM was diagnosed based on ventricular enlargement.

3.2. Statistical analysis

Two types of analyses were conducted to assess the relationship between ventricular enlargement and cortical folding. First, a global analysis, using both F_D and F_V, was performed to investigate the association of INSVM with cortical folding. Second, a hemispheric analysis was conducted, using the F_V model, where the effect of ventricular dilation was studied per hemisphere. In this last analysis, the relationship between ventricular dilation and cortical folding was studied per hemisphere. Therefore, the *VV* covariate represents the volume of the corresponding lateral ventricle.

Table 4 lists the cortical regions where significant differences in cortical folding related to INSVM diagnosis (F_D) or total ventricular enlargement (F_V) were found in at least one of the folding measures analyzed. We found that ventricular volume in Eq. (3) was more sensitive than diagnosis as shown in Table 4, reaching significance in more folding measures and cortical regions (i.e., occipital and parietal lobes). Moreover, when analyzing ipsilateral associations, ventricular volume showed a stronger effect on the cortical folding in the same hemisphere (see Table 5) when compared to the global model using total ventricular volume. In general, the cortical regions most associated with VM were insula, occipital and parietal lobes, and the regions located in the posterior part of the temporal lobe.

As shown in the last column of Table 4, whole hemispheres were included as single regions to check for global effects. In the whole hemisphere, diagnosis was not associated with any folding measure, while significantly lower values of PMC and MCL2 (all $p = .002$) associated with ventricular enlargement were found in the right hemisphere, and bilaterally higher values of NGC (left: $p = .002$, right: $p = .001$). At a regional basis, significant differences in PMC (left: $p < 10^{-4}$, right: $p < 10^{-5}$) and CI (left: $p < .0002$, right $p < 10^{-5}$), among others, were found bilaterally with both F_D and F_V models in GPApp and MITGpp, with diagnosis and ventricular dilation associated with a decreased cortical folding in all measures reaching significance. In the insula, significant effects of diagnosis were found in NMC ($p < .002$) and NGC ($p < .001$) solely in the right hemisphere. Ventricular volume was, however, associated with several folding measures in the right hemisphere and bilaterally with NGC (left: $p < .002$, right: $p < 10^{-5}$) and FI (both $p < .001$). Significant changes were also found by both F_D and F_V in GPAap and LOGFpp, although no curvature measure showed bilateral differences, with the exceptions of GPAap, where MC (both $p < .001$) and PMC (both $p < .001$) were bilaterally associated with ventricular enlargement. In association with abnormality, GPAap showed increased curvature. In LOGFpp, we found variable effects depending on the hemisphere and folding measure. Reduced cortical folding in the left SGTpp (i.e., increased NMC and NGC) was only found by the F_D. The second model (F_V), however, seemed to be more sensitive since significant folding differences in the occipital and parietal lobes were not detected in the first model (i.e., using diagnosis as factor, F_D). Increasing ventricular volume was significantly associated with bilateral gyrification decrease of the occipital lobe in multiple folding measures (e.g., NMC left: $p < .0002$, right: $p < 10^{-4}$). In the parietal lobe, ventricular volume was associated with reduced curvature in the left hemisphere and bilaterally only with PMC (left: $p < .0001$, right: $p = .002$).

Note that in this first analysis (using both F_D and F_V models), we assumed that diagnosis and ventricular enlargement might be associated with gyrification differences over the whole cortical plate, irrespective of its side. That is, the diagnosis used as group factor in F_D and the total ventricular volume in F_V could not distinguish the laterality. However, since there are cases diagnosed with left, right or bilateral INSVM in our abnormal cohort, we further conducted a second analysis to assess the association of ventricular dilation with reduced cortical

Table 4
Regions with statistically significant differences in cortical folding associated with diagnosis/ventricular enlargement. Abbreviations: left hemisphere (L), right hemisphere (R), bilateral (B), and hemisphere (Hem). The term before the forward slash indicates statistical significance found using the F_D model, while the one after the slash indicates significance when using F_V (i.e., F_D/F_V). Abbreviations L, R, and B represent that significance is found only in the left, right hemisphere, and bilaterally, respectively. When there is no statistical significance for one model, '–' is used. For example, the entry corresponding to GPAap and MC shows that the effect of diagnosis (i.e. F_D model) in the MC folding measure of the right GPAap is statistically significant, whereas it is not in the left GPAap. However, the effect of ventricular dilation (i.e., F_V) in both right and left GPAap is statistically significant.

	GPAap	GPApp	Ins	LOGFpp	MITGpp	OL	PL	STGpp	Hem
MC	R/B	B/B	–/R	–/R	R/R				
PMC	R/B	B/B			B/B	–/B	–/B		–/R
NMC			R/R	L/–	–/R	–/B		L/–	
GC	–/L			L/L		–/B			
PGC		B/B	–/R	L/–	L/B	–/B	–/L		
NGC		R/R	R/B		L/B	–/B	–/L	L/–	–/B
CI		B/B	–/R		B/B	–/B	–/L		
FI	–/L	B/B	–/B		B/B				
SI	–/L	–/R		R/R					
PSI	–/L	L/B		R/R					
NSI				L/R					
MCL2	–/L	B/B	–/R	L/–	B/B	–/B	–/L		–/R
GCL2		L/B		L/–	L/L	–/R			
MCNR		B/B		L/–	L/–	–/R			
GCNR		L/B				–/R			

Table 5
Regions with statistically significant differences in cortical folding associated with hemispheric ventricular enlargement. Abbreviations: left hemisphere (L), right hemisphere (R), bilateral (B), and hemisphere (Hem). Abbreviations R/L indicate that statistical significance is achieved only in the region of right/left hemisphere by the F_V model that only uses the right/left ventricular volume. When statistical significance is found by both hemispheric models on their respective sides, B is used.

	GPAap	GPApp	Ins	LOGFpp	MITGpp	OL	PL	STGpp	Hem
MC	B	B	B	R	B				
PMC	R	B			B	B	B		B
NMC	L		B	L	R	B	L		L
GC				L		B			
PGC		B	B	L	B	B	L		B
NGC		B	B		B	B	L		B
CI	R	B	B	L	B	B	B	R	B
FI		B	L		B	R			
SI	L	B		R					
PSI	L	B		R					
NSI	L	L		R		L			
MCL2		B	B	L	B	B	L		B
GCL2		B		L	R	R			
MCNR		B		L	R	B			
GCNR		B		L		R			

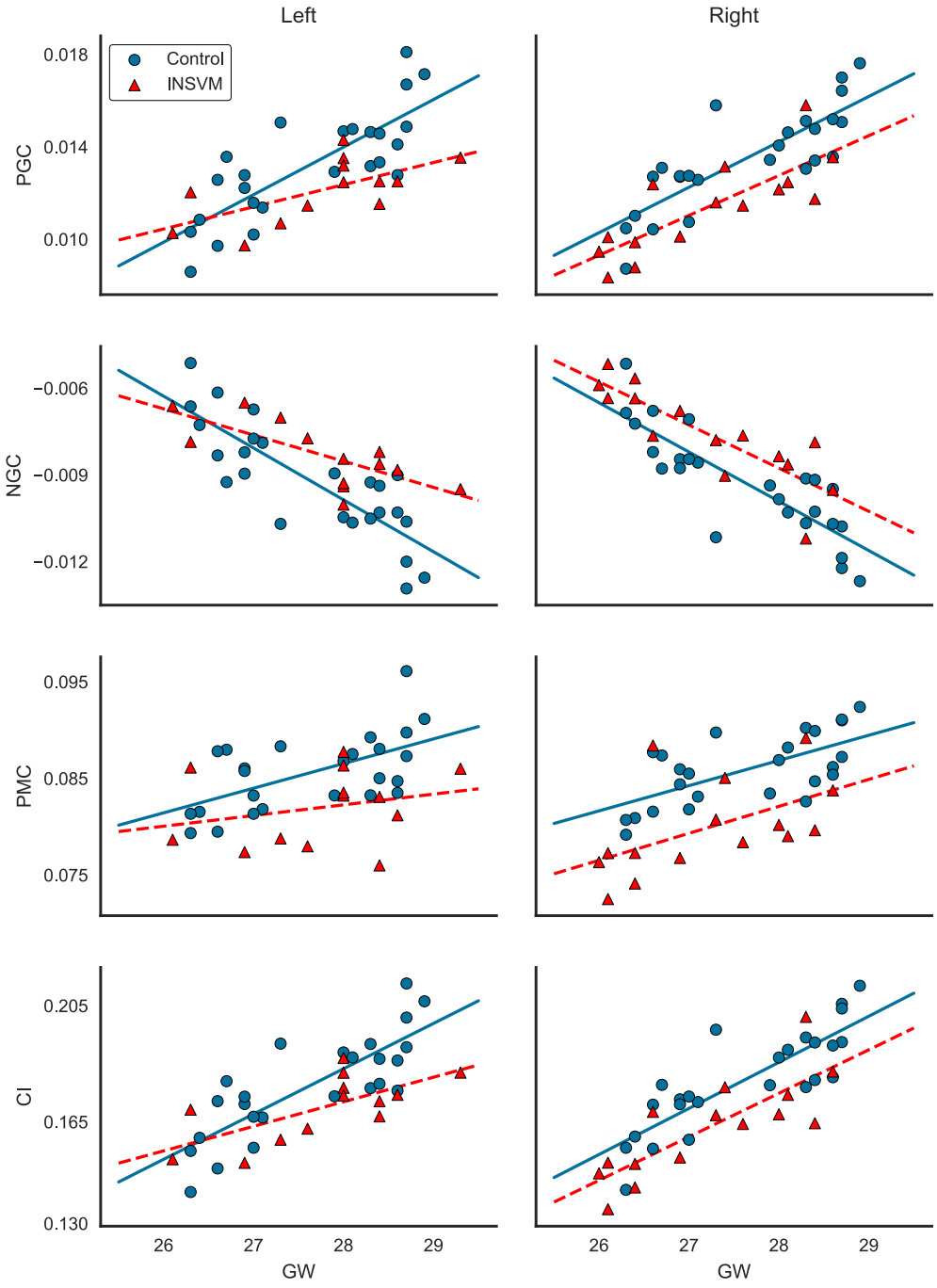

Fig. 5. Scatter plots of PGC, NGC, PMC and CI versus GA for each hemisphere, with linear fits for controls and subjects with left or right INSVM, depending on the hemisphere. Note that fetuses with bilateral ventricular enlargement appear as INSVM in both hemispheres.

folding for each hemisphere separately.

Results from this second hemispheric analysis are shown in Table 5. Cortical regions and folding measures statistically associated with ventricular volume show great overlap with the previous analysis using total ventricular volume (i.e., F_V), though it is important to emphasize the differences concerning the insula and whole hemisphere. In this second analysis, lateral ventricular dilation had a significant effect on reduced folding in both insula and whole hemisphere in the majority of curvature measures. Reductions in folding related bilaterally to NMC, PGC, NGC, CI and MCL2 were found in the insula, with increased curvature only observed in MC. Regarding the whole hemispheres, lateral ventricular volume was consistently correlated with reduced folding in all statistically significant curvature measures, with NGC rendering the lowest p-values (left: $p < 10^{-4}$ and right: $p = .0002$). Some of these measures are shown per hemisphere in Fig. 5. This suggests that albeit cortical folding might be bilaterally altered in the presence of unilateral ventricular enlargement, ipsilateral association is higher.

3.3. Ventricular volume prediction

Sparse linear models were used to predict total ventricular volume and identify the most relevant cortical regions and curvature-based features related to ventricular enlargement. Before regression, all features were scaled to a mean of 0 and a standard deviation of 1. Average mean absolute errors (MAE) using a leave-one-out cross-validation strategy for each value of λ in the range $[10^{1},10^{-4}]$ are shown in Fig. 6. The goal of this experiment is to choose the optimal value for the regularization parameter λ. This is, the optimal amount of regularization (i.e., sparsity) is chosen to be the one that leads to the lowest

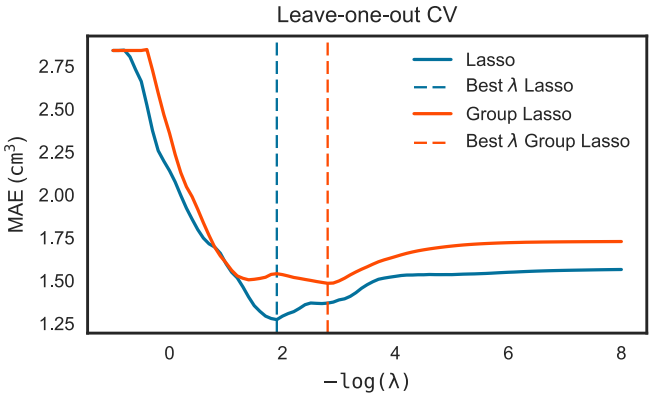

Fig. 6. Leave-one-out cross-validated mean absolute error evolution using different regularization values. Comparison of Lasso with Group Lasso.

ventricular volume prediction error. We can see that Lasso yields more accurate volume prediction than Group Lasso. Lasso is more free to choose the most relevant features from any cortical region, while Group Lasso is constrained to select groups of features (i.e., a group of features corresponds to a cortical region), except for GA and STV, which are single feature groups.

Fig. 7 shows the MAE for the optimal λ values corresponding to Lasso and Group Lasso, respectively, separated by cohort. For all fetuses, the MAE obtained is 1.27 cm^3 (control: 0.98, INSVM: 1.59) and 1.48 cm^3 (control: 1.20, INSVM: 1.79) for Lasso and Group Lasso, respectively. With 3.65 ± 1.12 cm^3 and 8.91 ± 2.70 cm^3 being the ventricular volumes in normal and INSVM cohorts, respectively. Note that both methods provided higher mean error in the INSVM cohort than in normal fetuses. This may be due to the large volume variance and heterogeneity (see Fig. 4) existing in the abnormal cohort (including left, right and bilateral INSVM).

The advantage of using sparse regularization is that most feature coefficients will be driven towards zero and only few relevant features will be selected. However, there may be some instability in the features selected by Lasso since they may vary depending on the data used to compute the model. To further assess the relevance of selected regions, stability selection was considered using Randomized Lasso. After training Lasso and Group Lasso with their respective best λ values on the complete dataset, and running Randomized Lasso, the percentage of features selected was: 6.02% (28 folding measures and STV), 50.21% (240 folding measures representing 16 cortical regions, GA and STV) and 6.02% (28 folding measures and STV) for Lasso, Group Lasso and Randomized Lasso, respectively. This shows that a few folding measures are relevant for predicting ventricular volume, according to the number of features selected by both Lasso and Randomized Lasso. Noteworthy is the fact that STV was selected by all sparse models, whereas GA was relevant for predicting ventricular volume only in Group Lasso.

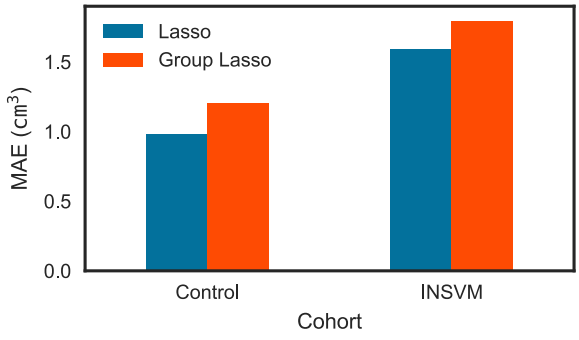

Fig. 7. Total ventricular volume mean absolute error in normal and INSVM cohorts: Comparison between Lasso and Group Lasso. Results are obtained with the optimal cross-validated λ for each method.

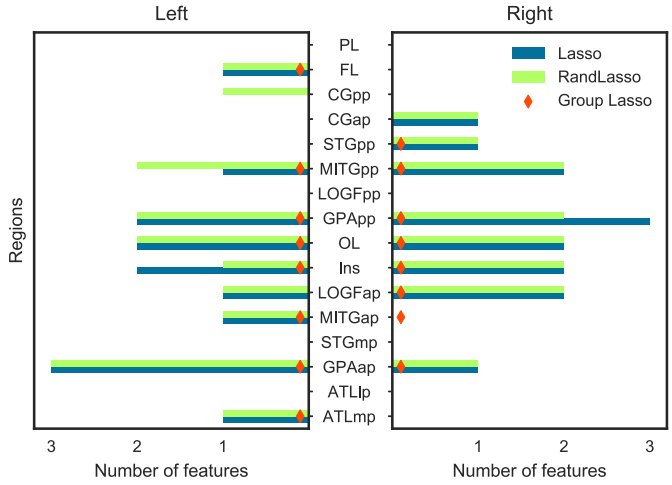

Fig. 8. Number of features selected from cortical regions considered by left and right hemisphere. Note that Group Lasso selects all curvature features from a particular region.

Although Fig. 4 shows a correlation between ventricular volume and GA, STV appears to better capture this association. This is because STV carries information about GA ($p < 10^{-12}$) and, most importantly, is highly sensitive to ventricular volume ($p < 10^{-6}$).

Fig. 8 shows the most relevant regions, in terms of number of features selected. It is important to note that MITGpp, GPAap, GPApp, occipital lobe and insula were selected bilaterally by all sparse models, which is in great accordance with our previous statistical analyses. However, in the parietal lobe, that showed significant association with ventricular volume enlargement, no curvature feature was selected by any regression model. This suggests that, although this region is correlated with ventricular enlargement, is not part of the predictive pattern obtained when considering all measures in conjunction. Curvature features selected by Lasso and Randomized Lasso are shown in Fig. 9. The most recurrent features (selected in more than 3 cortical regions by Lasso or Randomized Lasso) were MC, PMC, GC, SI and PSI. MC and PMC denote extrinsic folding differences between cortices of healthy fetuses and those of the INSVM cohort in the cortical regions were these folding measures were found relevant by our sparse estimators. MC was found relevant in the right insula, for example, which is predominantly more concave in the normal cohort than in INSVM fetuses with larger ventricles (as shown in Fig. 10). The left GPAap, however, was extrinsically less folded (lower MC) in INSVM subjects. In the right MITGpp, PMC was selected by both Lasso and Randomized Lasso because of its negative correlation with ventricular volume. The gyrus is more prominent in the normal cohort, as clearly illustrated in Fig. 10. The relevance of GC implies that there exists a difference in intrinsic folding (i.e., with distortion) between both cohorts in regions such as the left occipital lobe (where GC was found relevant). SI was found to be relevant, for example, in the right LOGFap and PSI in left GPAap.

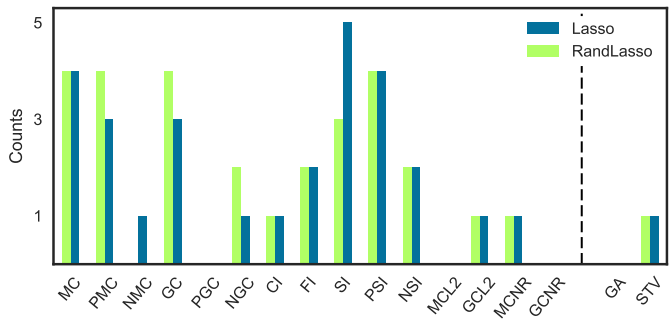

Fig. 9. Feature selection counts corresponding to the number of cortical regions where a particular curvature feature was selected.

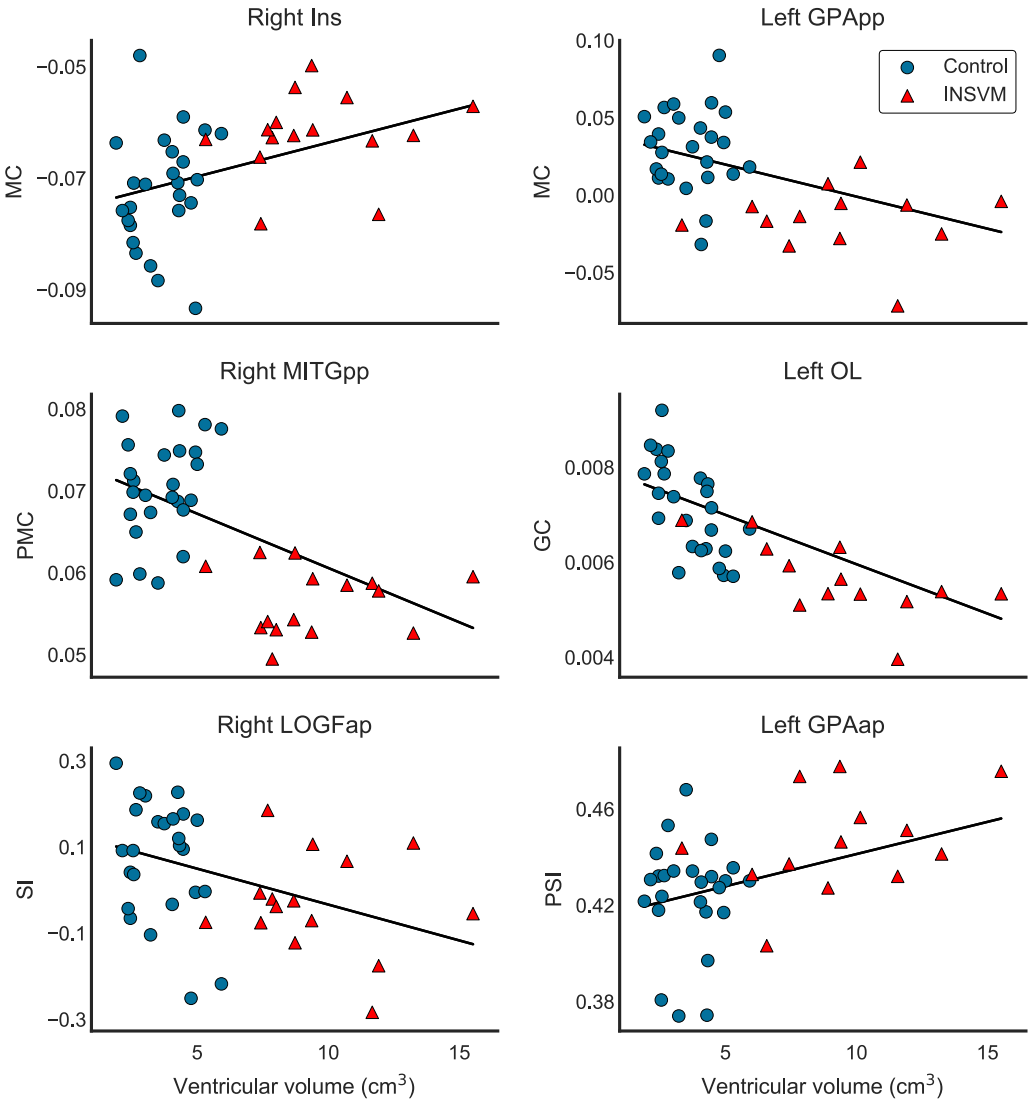

Fig. 10. Examples of folding measures (selected by our sparse models) against ventricular volume. Linear fit is included to show relationship of measures with increasing ventricular volume.

The former expresses that right LOGFap is, in general, more convex in healthy fetuses, while the latter points out to the existence of a less prominent convexity within the left GPAap. This, however, does not mean that other selected measures were not important. It simply indicates that the most recurrent measures were found to be strongly correlated with ventricular volume in several cortical regions, which emphasizes their predictive power and higher sensitivity over the rest of measures to capture the putative effects of INSVM in such regions. On the other hand, PGC, MCL2 and GCNR were not relevant for any cortical region, which may reflect that when used together with the rest of folding measures, they provided no additional information for our sparse models in the prediction of ventricular volume or were not able to capture folding differences between both cohorts. Despite some differences, results obtained with GLM analyses and sparse regression are concordant.

4. Discussion

In this work, we studied the association of INSVM with altered cortical folding *in utero*. Using high-quality 3D reconstructions of fetal brain MR images, inner cortical surfaces were extracted and several folding measures were computed to characterize the curvature and degree of gyrification of each fetal brain. Two different approaches based on statistical analysis and sparse linear regression were employed to identify cortical regions associated with ventricular dilation. In the first approach, we probed the capability of diagnosis or ventricular volume to explain the observed folding measure for each cortical region individually. We also corrected for other covariates (i.e., GA and supratentorial volume) that could affect the relationship to make sure that the differences are only due to diagnosis or ventricular volume. In the second approach, we aimed to find a pattern among the observed regions that is predictive of total ventricular volume. Such pattern is composed of several cortical regions and we considered that a region is relevant if it is included in such pattern. Both approaches offer complementary information since regions are either considered separately or in groups. We conclude that the regions that are significant in the statistical analysis and also selected by the sparse linear models can be considered to play an important role in gyrification in fetuses with INSVM. Both approaches showed evidence of disturbances in cortical folding in the presence of VM. Their results were in great accordance, with reduced folding in insula, MITGpp, GPApp and occipital lobe demonstrating consistent bilateral relationship with increasing ventricular volume.

4.1. Alterations in cortical folding

In the statistical analyses, ventricular volume was more sensitive to changes in folding than diagnosis, being able to capture differences in

additional regions (i.e., occipital and parietal lobes) and in the whole hemisphere. When cortical folding was analyzed separately for each hemisphere, there was an increased number of folding measures that significantly correlated with ventricular volume in the insula and occipital lobe in both hemispheres. This shows stronger associations of altered cortical folding with ipsilateral ventricular enlargement and underlines the importance of using hemispheric analyses. We argue this is because our dataset is composed of INSVM subjects with unilateral and bilateral ventricular dilation, and global analysis is not able to discern the laterality. Although this might suggest stronger ipsilateral effects of ventricular enlargement in cortical folding, a contralateral analysis might reveal interactions across different hemispheres. Cortical regions found relevant by the sparse linear models, emphasizing regions selected by Randomized Lasso, were in great overlap with regions significantly associated with ventricular volume in the statistical analyses, with the important exception of the parietal lobe. Although Randomized Lasso selected new cortical regions (e.g., left: CGpp, ATLmp and LOGFap, right: LOGFap and MITGap), it is worth mentioning that these regions might have been selected to account for the amount of ventricular volume not explained by the regions with reduced folding.

Based on 3D reconstructed MR images, Scott et al. (2013) used a vertex-wise approach to investigate the association of isolated mild ventriculomegaly (IMVM) with alterations in cortical folding. Significant deviations in mean curvature were only found in the anterior aspect of the parieto-occipital sulcus. On the contrary, in the current study, several cortical regions showed significantly lower values associated with INSVM in multiple folding measures (e.g., mean curvature, Gaussian curvature and curvedness). Our findings encompass the narrow area of the parieto-occipital sulcus that distinguished fetuses with IMVM from the normal cohort. Scott et al. (2013) analyzed folding alterations in fetuses with mild VM (i.e., atrial diameter of 10–12 mm) instead of INSVM that includes both mild and moderate VM. The inclusion of fetuses with larger lateral ventricular volumes in our cohort than the ones with IMVM may explain the additional regions with altered folding found in our study. Moreover, Scott et al. (2013) compared folding between 16 healthy controls and 16 IMVM fetuses, while our database is composed of 23 INSVM subjects and 25 controls.

According to sulcogenesis studies based on cortical surfaces (Habas et al., 2012; Clouchoux et al., 2012), the parieto-occipital sulcus, separating the parietal and occipital lobes, undergoes significant changes starting from the 23rd GW. In the occipital lobe, significant changes in curvature are found in the calcarine sulcus and lingual gyrus around the 24th GW and continue until they are well formed around 28–29 GWs. This might have precluded finding folding differences in these areas between controls and cases in Scott et al. (2013). The same occurs in the insula, for instance, where first significant folding changes are detected around 24–25 GWs. Between 22 and 25.5 GWs, the age range studied in Scott et al. (2013), most primary sulci are still emerging, which may difficult the detection of cortical alterations. The GA of our cohort is one of the factors that allowed us to identify gyrification differences in more cortical areas than only in the parieto-occipital sulcus. In normal *in utero* brain development, the age range of 26–29 GWs of our cohort constitutes a period of cortical folding that occurs immediately before gyrification reaches its peak of growth rate around the 30th GW in all cortical regions (Wright et al., 2014). By the end of this period, most primary gyri and sulci are formed in the developing brain.

Although folding differences in our work were analyzed at a regional scale, reduced folding in the aforementioned cortical regions hints to the existence of gyrification alterations that can be found in more localized areas confined within these regions.

4.2. Prognosis in INSVM fetuses

We know from several published studies assessing perinatal and long-term outcomes that the incidence of unfavorable neurodevelopmental outcome is low in INSVM fetuses, and even lower in mild than moderate VM (Gaglioti et al., 2005; Leitner et al., 2009; Griffiths et al., 2010). Within isolated VM, ventricular size and progressive ventricular enlargement are the main factors showing association with adverse outcome and postnatal cerebral abnormalities not detected *in utero* (Kelly et al., 2001; Gilmore et al., 2008; Baffero et al., 2015, Scala et al., 2017).

Neurodevelopmental impairment observed with postnatal assessment in fetuses diagnosed with INSVM include delays in cognitive, psychomotor and language skills (Leitner et al., 2009; Beeghly et al., 2010; Ouahba et al., 2006; Lyall et al., 2012). Risk of attention-deficit/hyperactivity disorder was also observed in children with prenatal non-severe VM (Gilmore et al., 2001; Ball et al., 2013). These functional deficits were also associated with abnormal cortical descriptors in a vast variety of disorders such as mental retardation (Zhang et al., 2010), attention-deficit/hyperactivity disorder (Wolosin et al., 2009) and schizophrenia (Jou et al., 2005; Powell, 2010). Fetuses with prenatally diagnosed INSVM showed larger cortical GM volume (Kyriakopoulou et al., 2014), which was also present in neonates along with alterations in WM (Gilmore et al., 2008; Lyall et al., 2012). The usefulness of cortical folding in predicting adverse outcome of fetuses with INSVM remains speculative and is yet to be evidenced by longitudinal and follow-up studies. Nonetheless, cortical folding has proved to be a potential predictor in preterm neonates (Moeskops et al., 2015), schizophrenia (Guo et al., 2015) and Alzheimer's disease (Cash et al., 2012).

Fetal MRI grants the means to obtain more detailed information of the *in utero* brain. With the recent advancements on motion-correction and super-resolution techniques, fetal MRI is becoming an important neuroimaging modality that offers the possibility to use a wide variety of approaches to study malformations during *in utero* neurodevelopment. For INSVM, using fetal MRI for the search of novel prognostic biomarkers that are able to elucidate the neurodevelopmental outcome of fetuses with non-severely dilated ventricles is essential to identify fetuses at higher risk of neurodevelopmental deficits. Cortical regions with significant convolutional alterations found in this study constitute potential candidate biomarkers that must be assessed in future follow-up studies to validate their prognostic or predictive power in distinguishing between the two subgroups of INSVM fetuses (i.e., INSVM fetuses with favorable and adverse outcome).

Still, the association of VM with decreased cortical folding and its effects in postnatal neurodevelopment remain poorly understood. Moreover, drawing conclusions about the direct influences of VM on gyrification, with the possible exception of cortical areas surrounding the dilated ventricles, is not straightforward since the etiology of VM remains unknown (Kelly et al., 2001) and there may be other common hidden factors that cause both lateral ventricular dilation and decreasing gyrification.

4.3. Limitations and future work

One limitation of the current study is the large extension of the cortical regions identified to be related to INSVM. Although cortical folding alterations were found in the whole hemispheres, reduced cortical folding in these regions (e.g., occipital lobe) could be concentrated in more focalized areas. Therefore, in order to find such specific areas, a vertex-wise analysis needs to be conducted. Regarding the cohorts, the study group was composed of fetuses diagnosed with mild or moderate VM and no distinction was made to assess the alterations in gyrification associated with each subgroup. However, this may not be considered a limitation since we analyzed the correlation with lateral ventricular volume instead of atrial diameter. Furthermore, from the neurodevelopmental perspective, there is no consensus in the literature on the differences between mild and moderate VM. Another limitation is the gender distribution in our cohorts. Our dataset is composed of 25 healthy controls (14 males, 11 females) and 23 INSVM subjects (21 males, 2 females), as shown in Table 1. This imbalance

between groups (i.e., male overrepresentation in the INSVM cohort, with only 2 females) has precluded studying the effect of gender. A further limitation comes from the automatic tissue segmentation. Only 4 images were manually delineated and used as atlases to segment the remaining 44 brain MR images. This might have affected our analyses, specially in the anterior part of the parahippocampal gyri, where segmentation could be improved.

In the current study, although only curvature-based folding measures were analyzed, other measures related with cortical folding such as gyrification index (Zilles et al., 1988) and sulcal depth can be studied. Given the existence of cortical folding alterations associated with INSVM, cortical thickness constitutes another measurement worth investigating. Future work also involves testing all folding measures and cortical regions associated with INSVM with follow-up data, using neonatal images and other information such as neurodevelopmental test scores. This may serve to select, among all these candidate cortical regions, the ones with altered folding that might be used as biomarkers to identify the fetuses with INSVM that will have poor outcome.

5. Conclusions

In this work, we studied *in utero* gyrification in the presence of non-severe ventricular enlargement. Our findings demonstrate a relationship of VM with reduced folding in several cortical regions, not only restricted to the parieto-occipital sulcus. Delving deeper into other *in utero* maturational processes that occur in the fetal brain, such as cortical folding, can shed light on other possible malformations that might lead to adverse neurodevelopment of INSVM fetuses. To the best of our knowledge, this is the first work to analyze INSVM-specific cortical folding alterations within the GA range of 26–29 weeks using 3D reconstructed fetal MRI.

Acknowledgements

This work was co-financed by the Marie Curie FP7-PEOPLE-2012-COFUND Action, Grant agreement no: 600387. This study was partly supported by Instituto de Salud Carlos III (PI16/00861) integrados en el Plan Nacional de I+D+I y cofinanciados por el ISCIII-Subdirección General de Evaluación y el Fondo Europeo de Desarrollo Regional (FEDER) “Una manera de hacer Europa”; additionally the research leading to these results has received funding from “la Caixa” Foundation, and The Cerebra Foundation for the Brain-Injured Child, Carmarthen, Wales.

Appendix A. Supplementary data

Supplementary data to this article can be found online at https://doi.org/10.1016/j.nicl.2018.01.006.

References

Avants, B.B., Epstein, C.L., Grossman, M., Gee, J.C., 2008. Symmetric diffeomorphic image registration with cross-correlation: evaluating automated labeling of elderly and neurodegenerative brain. Med. Image Anal. 12, 26–41. http://dx.doi.org/10.1016/j.media.2007.06.004.

Avants, B.B., Tustison, N.J., Wu, J., Cook, P.A., Gee, J.C., 2011. An open source multivariate framework for n-tissue segmentation with evaluation on public data. Neuroinformatics 9, 381–400. http://dx.doi.org/10.1007/s12021-011-9109-y.

Baffero, G.M., Crovetto, F., Fabietti, I., Boito, S., Fogliani, R., Fumagalli, M., Triulzi, F., Mosca, F., Fedele, L., Persico, N., 2015. Prenatal ultrasound predictors of postnatal major cerebral abnormalities in fetuses with apparently isolated mild ventriculomegaly. Prenat. Diagn. 35, 783–788. http://dx.doi.org/10.1002/pd.4607.

Ball, J.D., Abuhamad, A.Z., Mason, J.L., Burket, J., Katz, E., Deutsch, S.I., 2013. Clinical outcomes of mild isolated cerebral ventriculomegaly in the presence of other neurodevelopmental risk factors. J. Ultrasound Med. 32, 1933–1938. http://dx.doi.org/10.7863/ultra.32.11.1933.

Batchelor, P.G., Smith, A.D.C., Hill, D.L.G., Hawkes, D.J., Cox, T.C.S., Dean, A.F., 2002. Measures of folding applied to the development of the human fetal brain. IEEE Trans. Med. Imaging 21, 953–965. http://dx.doi.org/10.1109/TMI.2002.803108.

Batty, M.J., Palaniyappan, L., Scerif, G., Groom, M.J., Liddle, E.B., Liddle, P.F., Hollis, C., 2015. Morphological abnormalities in prefrontal surface area and thalamic volume in attention deficit/hyperactivity disorder. Psychiatry Res. Neuroimaging 233, 225–232. http://dx.doi.org/10.1016/j.pscychresns.2015.07.004.

Beeghly, M., Ware, J., Soul, J., du Plessis, A., Khwaja, O., Senapati, G.M., Robson, C.D., Robertson, R.L., Poussaint, T.Y., Barnewolt, C.E., Feldman, H.A., Estroff, J.A., Levine, D., 2010. Neurodevelopmental outcome of fetuses referred for ventriculomegaly. Ultrasound Obstet. Gynecol. 35, 405–416. http://dx.doi.org/10.1002/uog.7554.

Benkarim, O.M., Sanroma, G., Zimmer, V.A., Muñoz Moreno, E., Hahner, N., Eixarch, E., Camara, O., González Ballester, M.A., Piella, G., 2017. Toward the automatic quantification of in utero brain development in 3D structural MRI: a review. Hum. Brain Mapp. 38, 2772–2787. http://dx.doi.org/10.1002/hbm.23536.

Cardoza, J., Goldstein, R., Filly, R., 1988. Exclusion of fetal ventriculomegaly with a single measurement: the width of the lateral ventricular atrium. Radiol. 169, 711–714. http://dx.doi.org/10.1148/radiology.169.3.3055034.

Cash, D.M., Melbourne, A., Modat, M., Cardoso, M.J., Clarkson, M.J., Fox, N.C., Ourselin, S., 2012. Cortical Folding Analysis on Patients with Alzheimer's Disease and Mild Cognitive Impairment. Springer Berlin Heidelberg, Berlin, Heidelberg, pp. 289–296. http://dx.doi.org/10.1007/978-3-642-33454-2_36.

Clouchoux, C., Kudelski, D., Gholipour, A., Warfield, S., Viseur, S., Bouyssi-Kobar, M., Mari, J., Evans, A., du Plessis, A., Limperopoulos, C., 2012. Quantitative in vivo MRI measurement of cortical development in the fetus. Brain Struct. Funct. 217, 127–139. http://dx.doi.org/10.1007/s00429-011-0325-x.

Fernández, V., Llinares-Benadero, C., Borrell, V., 2016. Cerebral cortex expansion and folding: what have we learned? EMBO J. 35, 1021–1044. http://dx.doi.org/10.15252/embj.201593701.

Friedman, J., Hastie, T., Tibshirani, R., 2010. A Note on the Group Lasso and a Sparse Group Lasso. arXiv:1001.0736 ArXiv e-prints.

Gaglioti, P., Danelon, D., Bontempo, S., Mombr, M., Cardaropoli, S., Todros, T., 2005. Fetal cerebral ventriculomegaly: outcome in 176 cases. Ultrasound Obstet. Gynecol. 25, 372–377. http://dx.doi.org/10.1002/uog.1857.

Gholipour, A., Akhondi-Asl, A., Estroff, J., Warfield, S., 2012. Multi-atlas multi-shape segmentation of fetal brain MRI for volumetric and morphometric analysis of ventriculomegaly. NeuroImage 60, 1819–1831. http://dx.doi.org/10.1016/j.neuroimage.2012.01.128.

Gilmore, J.H., Smith, L.C., Wolfe, H.M., Hertzberg, B.S., Smith, J.K., Chescheir, N.C., Evans, D.D., Kang, C., Hamer, R.M., Lin, W., Gerig, G., 2008. Prenatal mild ventriculomegaly predicts abnormal development of the neonatal brain. Biol. Psychiatry 64, 1069–1076. http://dx.doi.org/10.1016/j.biopsych.2008.07.031.

Gilmore, J.H., van Tol, J.J., Streicher, H.L., Williamson, K., Cohen, S.B., Greenwood, R.S., Charles, H., Kliewer, M.A., Whitt, J., Silva, S.G., Hertzberg, B.S., Chescheir, N.C., 2001. Outcome in children with fetal mild ventriculomegaly: a case series. Schizophr. Res. 48, 219–226. http://dx.doi.org/10.1016/S0920-9964(00)00140-7.

Gómez-Arriaga, P., Herraiz, I., Puente, J.M., Zamora-Crespo, B., Núñez Enamorado, N., Galindo, A., 2012. Mid-term neurodevelopmental outcome in isolated mild ventriculomegaly diagnosed in fetal life. Fetal Diagn. Ther. 31, 12–18. http://dx.doi.org/10.1159/000331408.

Griffiths, P., Reeves, M., Morris, J., Mason, G., Russell, S., Paley, M., Whitby, E., 2010. A prospective study of fetuses with isolated ventriculomegaly investigated by antenatal sonography and in utero MR imaging. Am. J. Neuroradiol. 31, 106–111. http://dx.doi.org/10.3174/ajnr.A1767.

Guo, S., Iwabuchi, S., Balain, V., Feng, J., Liddle, P., Palaniyappan, L., 2015. Cortical folding and the potential for prognostic neuroimaging in schizophrenia. Br. J. Psychiatry 207, 458–459. http://dx.doi.org/10.1192/bjp.bp.114.155796.. arXiv:http://bjp.rcpsych.org/content/207/5/458.full.pdf.

Habas, P., Scott, J., Roosta, A., Rajagopalan, V., Kim, K., Rousseau, F., Barkovich, J., Glenn, O., Studholme, C., 2012. Early folding patterns and asymmetries of the normal human brain detected from in utero MRI. Cereb. Cortex 22, 13–25. http://dx.doi.org/10.1093/cercor/bhr053.

Hu, H.H., Chen, H.Y., Hung, C.I., Guo, W.Y., Wu, Y.T., 2013. Shape and curvedness analysis of brain morphology using human fetal magnetic resonance images in utero. Brain Struct. Funct. 218, 1451–1462. http://dx.doi.org/10.1007/s00429-012-0469-3.

Huisman, T.A.G.M., Tekes, A., Poretti, A., 2012. Brain malformations and fetal ventriculomegaly: what to look for? J. Pediatr. Neurol. 1, 185–195. http://dx.doi.org/10.3233/PNR-2012-028.

ISUOG Guidelines, 2007. Sonographic examination of the fetal central nervous system: guidelines for performing the ‘basic examination’ and the ‘fetal neurosonogram’. Ultrasound Obstet. Gynecol. 29, 109–116. http://dx.doi.org/10.1002/uog.3909.

Jou, R.J., Hardan, A.Y., Keshavan, M.S., 2005. Reduced cortical folding in individuals at high risk for schizophrenia: a pilot study. Schizophr. Res. 75, 309–313. http://dx.doi.org/10.1016/j.schres.2004.11.008.

Kelly, E.N., Allen, V.M., Seaward, G., Windrim, R., Ryan, G., 2001. Mild ventriculomegaly in the fetus, natural history, associated findings and outcome of isolated mild ventriculomegaly: a literature review. Prenat. Diagn. 21, 697–700. http://dx.doi.org/10.1002/pd.138.

Keraudren, K., Kuklisova-Murgasova, M., Kyriakopoulou, V., Malamateniou, C., Rutherford, M., Kainz, B., Hajnal, J., Rueckert, D., 2014. Automated fetal brain segmentation from 2D MRI slices for motion correction. NeuroImage 101, 633–643. http://dx.doi.org/10.1016/j.neuroimage.2014.07.023.

Klöppel, S., Abdulkadir, A., Jack, C.R., Koutsouleris, N., Mourão Miranda, J., Vemuri, P., 2012. Diagnostic neuroimaging across diseases. NeuroImage 61, 457–463. http://dx.doi.org/10.1016/j.neuroimage.2011.11.002.

Koenderink, J.J., van Doorn, A.J., 1992. Surface shape and curvature scales. Image Vis. Comput. 10, 557–564. http://dx.doi.org/10.1016/0262-8856(92)90076-F.

Kyriakopoulou, V., Vatansever, D., Elkommos, S., Dawson, S., McGuinness, A., Allsop, J., Molnár, Z., Hajnal, J., Rutherford, M., 2014. Cortical overgrowth in fetuses with

isolated ventriculomegaly. Cereb. Cortex 24, 2141–2150. http://dx.doi.org/10.1093/cercor/bht062.
Leitner, Y., Stolar, O., Rotstein, M., Toledano, H., Harel, S., Bitchonsky, O., Ben-Adani, L., Miller, E., Ben-Sira, L., 2009. The neurocognitive outcome of mild isolated fetal ventriculomegaly verified by prenatal magnetic resonance imaging. Am. J. Obstet. Gynecol. 201, 215.e1–215.e6. http://dx.doi.org/10.1016/j.ajog.2009.04.031.
Li, Y., Estroff, J.A., Mehta, T.S., Robertson, R.L., Robson, C.D., Poussaint, T.Y., Feldman, H.A., Ware, J., Levine, D., 2011. Ultrasound and MRI of fetuses with ventriculomegaly: can cortical development be used to predict postnatal outcome? Am. J. Roentgenol. 196, 1457–1467. http://dx.doi.org/10.2214/AJR.10.5422.
Lorensen, W.E., Cline, H.E., 1987. Marching cubes: a high resolution 3D surface construction algorithm. Comput. Graph. 21, 163–169. http://dx.doi.org/10.1145/37401.37422.
Lyall, A.E., Woolson, S., Wolfe, H.M., Goldman, B.D., Reznick, J.S., Hamer, R.M., Lin, W., Styner, M., Gerig, G., Gilmore, J.H., 2012. Prenatal isolated mild ventriculomegaly is associated with persistent ventricle enlargement at ages 1 and 2. Early Hum. Dev. 88, 691–698. http://dx.doi.org/10.1016/j.earlhumdev.2012.02.003.
Lyoo, I.K., Noam, G.G., Lee, C.K., Lee, H.K., Kennedy, B.P., Renshaw, P.F., 1996. The corpus callosum and lateral ventricles in children with attention-deficit hyperactivity disorder: a brain magnetic resonance imaging study. Biol. Psychiatry 40, 1060–1063. http://dx.doi.org/10.1016/S0006-3223(96)00349-6.
Makropoulos, A., Gousias, I., Ledig, C., Aljabar, P., Serag, A., Hajnal, J., Edwards, A., Counsell, S., Rueckert, D., 2014. Automatic whole brain MRI segmentation of the developing neonatal brain. IEEE Trans. Med. Imaging 33, 1818–1831. http://dx.doi.org/10.1109/TMI.2014.2322280.
Meinshausen, N., Bühlmann, P., 2010. Stability selection. J. R. Stat. Soc. Ser. B (Stat Methodol.) 72, 417–473. http://dx.doi.org/10.1111/j.1467-9868.2010.00740.x.
Melchiorre, K., Bhide, A., Gika, A.D., Pilu, G., Papageorghiou, A.T., 2009. Counseling in isolated mild fetal ventriculomegaly. Ultrasound Obstet. Gynecol. 34, 212–224. http://dx.doi.org/10.1002/uog.7307.
Moeskops, P., Benders, M.J.N.L., Kersbergen, K.J., Groenendaal, F., de Vries, L.S., Viergever, M.A., Igum, I., 2015. Development of cortical morphology evaluated with longitudinal MR brain images of preterm infants. PLOS ONE 10, 1–22. http://dx.doi.org/10.1371/journal.pone.0131552.
Murgasova, M., Quaghebeur, G., Rutherford, M., Hajnal, J., Schnabel, J., 2012. Reconstruction of fetal brain MRI with intensity matching and complete outlier removal. Med. Image Anal. 16, 1550–1564. http://dx.doi.org/10.1016/j.media.2012.07.004.
Mwangi, B., Tian, T.S., Soares, J.C., 2014. A review of feature reduction techniques in neuroimaging. Neuroinformatics 12, 229–244. http://dx.doi.org/10.1007/s12021-013-9204-3.
Ouahba, J., Luton, D., Vuillard, E., Garel, C., Gressens, P., Blanc, N., Elmaleh, M., Evrard, P., Oury, J., 2006. Prenatal isolated mild ventriculomegaly: outcome in 167 cases. BJOG Int. J. Obstet. Gynaecol. 113, 1072–1079. http://dx.doi.org/10.1111/j.1471-0528.2006.01050.x.
Pienaar, R., Fischl, B., Caviness, V., Makris, N., Grant, P., 2008. A methodology for analyzing curvature in the developing brain from preterm to adult. Int. J. Imaging Syst. Technol. 18, 42–68. http://dx.doi.org/10.1002/ima.v18:1.
Powell, S.B., 2010. Models of neurodevelopmental abnormalities in schizophrenia. Curr. Top. Behav. Neurosci. 4, 435–481. http://dx.doi.org/10.1007/7854_2010_57.
Rehn, A.E., Rees, S.M., 2005. Investigating the neurodevelopmental hypothesis of schizophrenia. Clin. Exp. Pharmacol. Physiol. 32, 687–696. http://dx.doi.org/10.1111/j.1440-1681.2005.04257.x.
Robinson, H.P., Fleming, J.E.E., 1975. A critical evaluation of sonar crown-rump length measurements. BJOG Int. J. Obstet. Gynaecol. 82 (9), 702–710. http://dx.doi.org/10.1111/j.1471-0528.1975.tb00710.x.
Rodriguez-Carranza, C., Mukherjee, P., Vigneron, D., Barkovich, J., Studholme, C., 2008. A framework for in vivo quantification of regional brain folding in premature neonates. NeuroImage 41, 462–478. http://dx.doi.org/10.1016/j.neuroimage.2008.01.008.
Rutherford, M., 2001. MRI of the Neonatal Brain. www.mrineonatalbrain.com.
Sadan, S., Malinger, G., Schweiger, A., Lev, D., Lerman-Sagie, T., 2007. Neuropsychological outcome of children with asymmetric ventricles or unilateral mild ventriculomegaly identified in utero. BJOG Int. J. Obstet. Gynaecol. 114, 596–602. http://dx.doi.org/10.1111/j.1471-0528.2007.01301.x.
Salomon, L.J., Bernard, J.P., Ville, Y., 2007. Reference ranges for fetal ventricular width: a non-normal approach. Ultrasound Obstet. Gynecol. 30, 61–66. http://dx.doi.org/10.1002/uog.4026.
Sanroma, G., Benkarim, O.M., Piella, G., González Ballester, M.A., 2016. Building an ensemble of complementary segmentation methods by exploiting probabilistic estimates. In: MICCAI Workshop on Machine Learning in Medical Imaging, pp. 27–35. http://dx.doi.org/10.1007/978-3-319-47157-0_4.
Scala, C., Familiari, A., Pinas, A., Papageorghiou, A.T., Bhide, A., Thilaganathan, B., Khalil, A., 2017. Perinatal and long-term outcomes in fetuses diagnosed with isolated unilateral ventriculomegaly: systematic review and meta-analysis. Ultrasound Obstet. Gynecol. 49, 450–459. http://dx.doi.org/10.1002/uog.15943.
Schaer, M., Cuadra, M.B., Tamarit, L., Lazeyras, F., Eliez, S., Thiran, J.P., 2008. A surface-based approach to quantify local cortical gyrification. IEEE Trans. Med. Imaging 27 (2), 161–170. http://dx.doi.org/10.1109/TMI.2007.903576.
Scott, J., Habas, P., Rajagopalan, V., Kim, K., Barkovich, A., Glenn, O., Studholme, C., 2013. Volumetric and surface-based 3D MRI analyses of fetal isolated mild ventriculomegaly. Brain Struct. Funct. 218, 645–655. http://dx.doi.org/10.1007/s00429-012-0418-1.
Shimizu, Y., Yoshimoto, J., Toki, S., Takamura, M., Yoshimura, S., Okamoto, Y., Yamawaki, S., Doya, K., 2015. Toward probabilistic diagnosis and understanding of depression based on functional MRI data analysis with logistic group lasso. PLOS ONE 10, 1–23. http://dx.doi.org/10.1371/journal.pone.0123524.
Shimony, J.S., Smyser, C.D., Wideman, G., Alexopoulos, D., Hill, J., Harwell, J., Dierker, D., Van Essen, D.C., Inder, T.E., Neil, J.J., 2016. Comparison of cortical folding measures for evaluation of developing human brain. NeuroImage 125, 780–790. http://dx.doi.org/10.1016/j.neuroimage.2015.11.001.
Studholme, C., Rousseau, F., 2014. Quantifying and modelling tissue maturation in the living human fetal brain. Int. J. Dev. Neurosci. 32, 3–10. http://dx.doi.org/10.1016/j.ijdevneu.2013.06.006.
Tibshirani, R., 1994. Regression shrinkage and selection via the lasso. J. R. Stat. Soc. Ser. B 58, 267–288.
Van Essen, D.C., Drury, H.A., 1997. Structural and functional analyses of human cerebral cortex using a surface-based atlas. J. Neurosci. 17, 7079–7102.
Vita, A., Dieci, M., Silenzi, C., Tenconi, F., Giobbio, G.M., Invernizzi, G., 2000. Cerebral ventricular enlargement as a generalized feature of schizophrenia: a distribution analysis on 502 subjects. Schizophr. Res. 44, 25–34. http://dx.doi.org/10.1016/S0920-9964(99)00134-6.
Wang, H., Suh, J.W., Das, S.R., Pluta, J.B., Craige, C., Yushkevich, P.A., 2013. Multi-atlas segmentation with joint label fusion. IEEE Trans. Pattern Anal. Mach. Intell. 35, 611–623. http://dx.doi.org/10.1109/TPAMI.2012.143.
Wolosin, S.M., Richardson, M.E., Hennessey, J.G., Denckla, M.B., Mostofsky, S.H., 2009. Abnormal cerebral cortex structure in children with ADHD. Hum. Brain Mapp. 30, 175–184. http://dx.doi.org/10.1002/hbm.20496.
Wright, I.C., Rabe-Hesketh, S., Woodruff, P.W., David, A.S., Murray, R.M., Bullmore, E.T., 2000. Meta-analysis of regional brain volumes in schizophrenia. Am. J. Psychiatr. 157, 16–25. http://dx.doi.org/10.1176/ajp.157.1.16.
Wright, R., Kyriakopoulou, V., Ledig, C., Rutherford, M., Hajnal, J., Rueckert, D., Aljabar, P., 2014. Automatic quantification of normal cortical folding patterns from fetal brain MRI. NeuroImage 91, 21–32. http://dx.doi.org/10.1016/j.neuroimage.2014.01.034.
Wright, R., Makropoulos, A., Kyriakopoulou, V., Patkee, P., Koch, L., Rutherford, M., Hajnal, J., Rueckert, D., Aljabar, P., 2015. Construction of a fetal spatio-temporal cortical surface atlas from in utero MRI: application of spectral surface matching. NeuroImage 120, 467–480. http://dx.doi.org/10.1016/j.neuroimage.2015.05.087.
Wu, J., Awate, S., Licht, D., Clouchoux, C., du Plessis, A., Avants, B., Vossough, A., Gee, J., Limperopoulos, C., 2015. Assessment of MRI-based automated fetal cerebral cortical folding measures in prediction of gestational age in the third trimester. Am. J. Neuroradiol. 36, 1369–1374. http://dx.doi.org/10.3174/ajnr.A4357.. arXiv:http://www.ajnr.org/content/36/7/1369.full.pdf.
Yuan, M., Lin, Y., 2006. Model selection and estimation in regression with grouped variables. J. R. Stat. Soc. Ser. B (Stat Methodol.) 68, 49–67. http://dx.doi.org/10.1111/j.1467-9868.2005.00532.x.
Zhang, Y., Zhou, Y., Yu, C., Lin, L., Li, C., Jiang, T., 2010. Reduced cortical folding in mental retardation. Am. J. Neuroradiol. 31, 1063–1067. http://dx.doi.org/10.3174/ajnr.A1984.
Zilles, K., Armstrong, E., Schleicher, A., Kretschmann, H.J., 1988. The human pattern of gyrification in the cerebral cortex. Anat. Embryol. 179, 173–179. http://dx.doi.org/10.1007/BF00304699.